JOURNAL OF GUIDANCE, CONTROL, AND DYNAMICS
Vol. 29, No. 3, May–June 2006

Proximity Operations of Formation-Flying Spacecraft Using an Eccentricity/Inclination Vector Separation

Simone D'Amico* and Oliver Montenbruck†
DLR, German Space Operations Center, 82230 Wessling, Germany

The implementation of synthetic apertures by means of a distributed satellite system requires tight control of the relative motion of the participating satellites. This paper investigates a formation-flying concept able to realize the demanding baselines for aperture synthesis, while minimizing the collision hazard associated with proximity operations. An elegant formulation of the linearized equations of relative motion is discussed and adopted for satellite formation design. The concept of eccentricity/inclination-vector separation, originally developed for geostationary satellites, is here extended to low-Earth-orbit (LEO) formations. It provides immediate insight into key aspects of the relative motion and is particularly useful for orbit control purposes and proximity analyses. The effects of the relevant differential perturbations acting on an initial nominal configuration are presented, and a fuel-efficient orbit control strategy is designed to maintain the target separation. Finally, the method is applied to a specific LEO formation (TanDEM-X/TerraSAR-X), and realistic simulations clearly show the simplicity and effectiveness of the formation-flying concept.

Nomenclature

A = reference area for drag computation
a = semimajor axis
B = effective baseline
b = ballistic coefficient
C_D = drag coefficient
D = relative difference operator, $\Delta_2 - \Delta_1$
e = eccentricity
$\boldsymbol{e}_N$ = unit vector in cross-track direction
$\boldsymbol{e}_R$ = unit vector in radial direction
$\boldsymbol{e}_T$ = unit vector in along-track direction
i = inclination
J_2 = geopotential second-order zonal coefficient
k = integer counter
M = mean anomaly
m = satellite mass
N = vertices of spherical triangles
$R_\oplus$ = Earth equatorial radius
$\boldsymbol{r}$ = satellite position
T = orbital period
T_e = period of the relative eccentricity vector motion
T_M = maneuver cycle
t = time
u = mean argument of latitude
$\boldsymbol{v}$ = satellite velocity
Δ = difference operator
$\Delta\boldsymbol{e}$ = relative eccentricity vector
$\Delta\boldsymbol{i}$ = relative inclination vector
δe = relative eccentricity vector modulus
δi = relative inclination vector modulus
ε = differential ballistic coefficient
θ = relative ascending node
ρ = atmospheric density
υ = true anomaly
φ = relative perigee
Ω = right ascension of the ascending node
ω = argument of perigee

Subscript and Superscripts

j = satellite designating number
t = target relative orbital element
1 = maneuver designating number

Received 15 December 2004; revision received 2 March 2005; accepted for publication 6 March 2005.

*Young Scientist, Flight Dynamics Group.
†Head, GPS Technology and Navigation Group.

Introduction

ONE of the objectives of current formation-flying research is to demonstrate that the satellites can be flown in a precise formation both by ground control and in an autonomous mode.[1] Even though ambitious formation-flying missions in low Earth orbit have been studied throughout the past decade[2] and many efforts are made in this area of spaceflight dynamics,[3] the practical experience is still limited to short-term proximity operations conducted mostly in the context of the manned space program. GRACE (Gravity Recovery and Climate Experiment), the closest low Earth orbit (LEO) formation in orbit right now, operates at a separation of 200 ± 50 km at 450 km altitude.[4] The EO-1 (Earth-Observing-1)/Landsat formation-flying demonstration was carried out at 700 km altitude with a separation of 450 ± 85 km over a five-month time span.[5] Both missions require only infrequent orbit adjustment maneuvers and allow for a convenient ground control to compensate differential drag effects.

The reason for such a gap between theoretical studies and real applications is that the benefits of satellites flying in formation come at a cost. The new systems architecture poses challenges in the areas of onboard sensing and actuation, high-level mission management and planning, as well as distributed fault detection and recovery.[6]

This paper presents a formation-flying concept for close LEO satellites (baseline <1 km) aiming to achieve the mission objectives, while minimizing collision risk and system complexity. The main focus is the realization of a space-borne synthetic-aperture-radar (SAR) interferometer[7] unaffected by temporal decorrelation, representative of repeat pass interferometry missions (e.g., Envisat, ERS), or by limited baseline lengths (e.g., X-SAR/SRTM Shuttle Topography mission). Because following arbitrary trajectories generally requires prohibitive amounts of fuel,[8] the goal is to develop fuel-efficient relative spacecraft trajectories that are useful for synthesizing scientific instruments. Because thruster activities have to be minimized to maximize the available time for SAR data collection, these trajectories are thrust-free and are referred to as passive apertures.[3]

The passive apertures have previously been designed using the periodic solutions to the Hill–Clohessy–Wiltshire (HCW) equations.[9] These equations describe the relative motion of two relatively close satellites flying in near circular orbits under the attraction of a main body. The HCW equations do not include any disturbance forces and as a consequence neglect completely the Earth's oblateness J_2 perturbations that have significant impact on the flight dynamics of LEO formations.[10] Considerable research has been performed into the development of models that incorporate J_2 effects.[11] The forces as a result of the Earth's oblateness are usually linearized, time averaged, and included in the HCW equations, but the short periodic perturbations are frequently ignored.[12]

In this study a practical approach to formation-flying design is taken by investigating a set of relative orbital elements that is more geometric in nature than the standard position and velocity component state vector. Some work has been done in the past on using orbital element differences[13,14] but the level of abstraction is still prominent and does not provide immediate insight into important aspects of the relative motion. The goal of this paper is to exploit the technique of eccentricity/inclination (e/i)-vector separation, which has originally been developed for geostationary satellites,[15] and extend the methodology to formation-flying design and control. To this end, the concept of eccentricity and inclination vectors is introduced, and a formulation suitable for LEO satellites is established. The relative motion is then described in terms of the relative e/i vectors. By considering the effect of short periodic perturbations, the formulation in terms of differential orbital elements can even be employed in the case of large along-track separations. It is therefore particularly useful in the buildup phase of a formation or the planning of longitude shift maneuvers.[16]

The paper provides a technical description of the proposed concept. After a discussion of the relative motion model, the relevant orbital perturbations are analyzed. Although the periodic perturbations are essentially cancelled for satellites operating in close proximity, the secular changes of the relative e/i vectors tend to disturb an initial nominal configuration. An appropriate orbit control strategy is therefore designed, to stabilize the relative motion at an affordable expenditure in terms of thruster activations and propellant consumption. The analytical treatment is validated by means of realistic simulations applied to a significant study case within the German national space program: the TanDEM-X/TerraSAR-X (TDX/TSX) formation-flying mission.[17]

Unperturbed Relative Motion

In this section a description of the relative motion of close spacecraft in near circular orbits is obtained from an analytical treatment of the Keplerian equations of motion. The goal of the following brief development is to describe the relative motion in terms of orbital elements differences and introduce the definitions of eccentricity and inclination relative vectors as a straightforward way to express the linearized equations of motion. The orbit of the jth spacecraft ($j = 1,2$) within the formation is represented in the Earth-centered-inertial (ECI) reference frame by the Keplerian orbital elements (a_j, e_j, i_j, Ω_j, ω_j, u_j), which correspond to the semimajor axis, eccentricity, inclination, right ascension of the ascending node, argument of perigee, and mean argument of latitude (i.e., $u_j = \omega_j + M_j$, where M_j is the mean anomaly), respectively. However, the ECI frame does not appear appropriate for the analysis of satellite relative motion. This is because a change of a single Keplerian element, like the orbital inclination, maps into all (x, y, z) axes for arbitrarily inclined orbital planes. A natural basis for inertial measurements and scientific observations is instead the orbital frame reference system that is given as the comoving triad, defined by the unit vector $\boldsymbol{e}_R$ along the radial direction (positive outwards), the unit vector $\boldsymbol{e}_T$ in along-track (tangential) direction of the satellite motion, and the unit vector $\boldsymbol{e}_N$ normal to the orbital plane in direction to the positive angular momentum vector (cross track). This triad denotes a right-handed system, with two time-dependent vectors $\boldsymbol{e}_R$ and $\boldsymbol{e}_T$, while $\boldsymbol{e}_N$ is time invariant in the Keplerian approximation.

The relative motion of spacecraft-2 (chaser) with respect to spacecraft-1 (master) can be expressed in the orbital frame centered on the master satellite as

$$\Delta\boldsymbol{r} = \boldsymbol{r}_2 - \boldsymbol{r}_1 = \Delta r_R \boldsymbol{e}_R + \Delta r_T \boldsymbol{e}_T + \Delta r_N \boldsymbol{e}_N \tag{1}$$

where $\boldsymbol{r}_j$ denotes the location of the participating satellites (Fig. 1) and $\Delta\bullet$ represents the operator difference ($\bullet_2 - \bullet_1$).

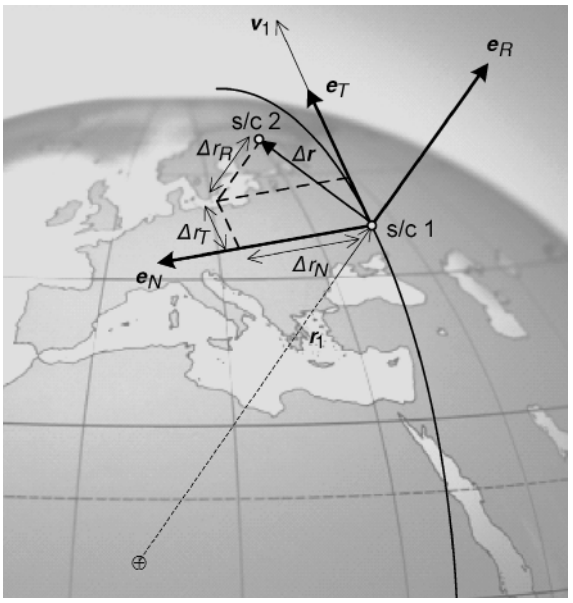

Fig. 1 Relative motion vector mapped into the orbital frame of s/c-1.

Linearization Assumptions

In contrast to an elaborate numerical integration of the orbit followed by a subsequent differencing of individual trajectories, the equation of motion for the two-body problem can directly be differenced.[18] Two assumptions are used to derive an appropriate relative motion model. First, the spacecraft are assumed to fly in near-circular orbits (i.e., $e_j \ll 1$). Second, they are taken sufficiently close to each other to justify the linearization of the equations of relative motion. The assumption of close formation flying can be translated into a small deviation of the nondimensional state vector of the chaser with respect to the nondimensional state vector of the master (i.e., $\|\Delta\boldsymbol{x}\| = \|(\Delta a/a_1, \Delta e, \Delta i, \Delta\Omega, \Delta\omega, \Delta u)\|^T \ll 1$).

In this case the compound relative motion scenario given by several Keplerian elements differing can be treated to first order by a linear superposition of the individual contributions. As a consequence, the in-plane ($\boldsymbol{e}_R$ and $\boldsymbol{e}_T$) and out-of-plane $\boldsymbol{e}_N$ relative motions are decoupled and can be expressed separately.[9]

Relative Inclination Vector and out-of-Plane Motion

A particularly straightforward case is the description of the relative motion of two satellites caused by variations in the inclination Δi and right ascension of the ascending node $\Delta\Omega$. Simple geometrical considerations (Fig. 2) suggest adopting the angle enclosed by the two orbital planes δi and the argument of latitude θ at which spacecraft-2 crosses the orbital plane of spacecraft-1 in ascending direction (i.e., the relative ascending node) to define a relative inclination vector as

$$\Delta\boldsymbol{i} = \begin{Bmatrix} \Delta i_X \\ \Delta i_Y \end{Bmatrix} = \sin(\delta i) \begin{Bmatrix} \cos\theta \\ \sin\theta \end{Bmatrix} \tag{2}$$

Let us now consider the sphere of radius $a_1 = a_2 = a$ centered on the Earth's center of mass (Fig. 2).

As it can be recognized from the law of sines and cosines for the spherical triangle with vertices N_1, N_2, and N_{12} (i.e., the absolute and relative ascending nodes), definition (2) simplifies to

$$\Delta\boldsymbol{i} \approx \begin{Bmatrix} \Delta i \\ \Delta\Omega \sin i \end{Bmatrix} \tag{3}$$

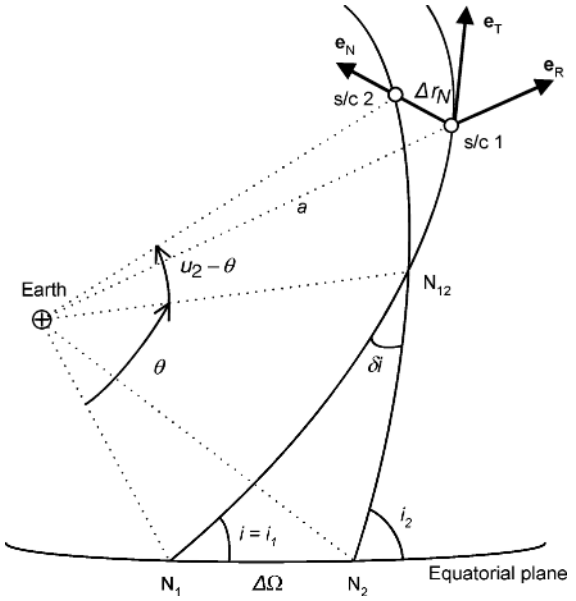

Fig. 2 Spherical triangles for the relative inclination vector definition.

for small differences in the orbital elements. Rigorously, i is the inclination of spacecraft-1 (i.e., $i \equiv i_1$), but can be likewise substituted by i_2 in the frame of our first-order theory. In the sequel the omission of the satellite designating subscript ($j = 1, 2$) indicates that the orbital elements of both satellites can be used equivalently. It is possible to apply the law of sines to the spherical triangle with vertices s/c 1, s/c 2, and N_{12}, to get a first-order approximation of the relative motion in cross-track direction:

$$\Delta r_N/a \approx \sin(u_2 - \theta)\sin(\delta i) \approx (-\Delta i_Y)\cos u + (\Delta i_X)\sin u \quad (4)$$

We will make use of the simplified representation given by Eq. (3) to study the effects of the orbital perturbations on the relative inclination vector and thus on the out-of-plane relative motion.

Relative Eccentricity Vector and in-Plane Motion

For near-circular satellite orbits, the Keplerian elements eccentricity and argument of perigee are commonly replaced by the eccentricity vector

$$\boldsymbol{e} = \begin{Bmatrix} e_X \\ e_Y \end{Bmatrix} = e \cdot \begin{Bmatrix} \cos\omega \\ \sin\omega \end{Bmatrix} \quad (5)$$

It is free from singularities and well suited for the study of orbital perturbations of remote sensing satellites.[19] The relative motion of two satellites as a result of variations in the eccentricity Δe and argument of perigee $\Delta\omega$ is easily described by introducing the difference

$$\Delta\boldsymbol{e} = \boldsymbol{e}_2 - \boldsymbol{e}_1 = \begin{Bmatrix} \Delta e_X \\ \Delta e_Y \end{Bmatrix} = \delta e \begin{Bmatrix} \cos\varphi \\ \sin\varphi \end{Bmatrix} \quad (6)$$

for two spacecraft (Fig. 3).

As it can be recognized by the harmonic expansion of the Kepler problem,[20] this so-called relative eccentricity vector characterizes the periodic relative motion within the orbital plane. It can be shown that for near-circular orbits the difference between true anomaly υ and mean anomaly is given by

$$\upsilon - M = 2e\sin M = (-2e_Y)\cos u + (2e_X)\sin u \quad (7)$$

whereas the radius r can be expressed as

$$r/a = 1 - e\cos M = (-e_X)\cos u - e_Y \sin u \quad (8)$$

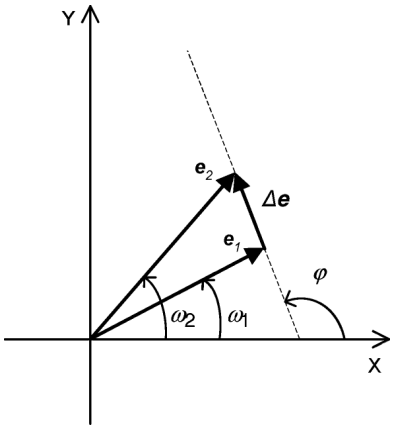

Fig. 3 Relative eccentricity vector definition.

Differencing Eqs. (7) and (8) between two satellites in close proximity with identical mean argument of latitude then yields

$$\Delta r_T/a \approx (\upsilon_2 - M_2) - (\upsilon_1 - M_1) = (-2\Delta e_Y)\cos u + (2\Delta e_X)\sin u \quad (9)$$

and equivalently

$$\Delta r_R/a \approx (r_2 - r_1)/a = (-\Delta e_X)\cos u - (\Delta e_Y)\sin u \quad (10)$$

Variations of Semimajor Axis and Argument of Latitude

Aside from the eccentricity and inclination vector difference, the relative motion of two spacecraft is affected by differences in the semimajor axis Δa and the mean argument of latitude Δu. For near-circular orbits, the semimajor axis change results in a systematic offset of size Δa in radial direction and in a secular tangential component given by $-\frac{3}{2}\Delta a(u - u_0)$, where $u_0 = u(t_0)$ is the argument of latitude at the epoch t_0. Thus, over a one-orbit period, the along-track separation accumulates to the amplitude of $-3\pi\Delta a$. Variations in the mean argument of latitude instead generate a tangential position offset of size $a\Delta u$ for near-circular orbits. The relative motion induced by Δa and Δu is given to first-order as

$$\Delta r_T/a \approx \Delta u - \tfrac{3}{2}(\Delta a/a)(u - u_0) \quad (11)$$

and

$$\Delta r_R/a \approx \Delta a/a \quad (12)$$

Linearized Equations of Relative Motion

Equations (4) and (9–12) show essentially that the relative motion can be decomposed into a harmonic oscillation perpendicular to the orbital plane and an elliptic in-plane motion, determined by the size and phase of the vectors $\Delta\boldsymbol{i}$ and $\Delta\boldsymbol{e}$. Superimposed to this, the radial and along-track separation show systematic offsets and a linear drift caused by Δa and Δu. Differentiation of these equations with respect to time yields the comprehensive linearized equations for the state vector (i.e., position and velocity) of spacecraft-2 in the orbital frame of the master[16]:

$$\begin{Bmatrix} \Delta r_R/a \\ \Delta r_T/a \\ \Delta r_N/a \\ \Delta \dot r_R/v \\ \Delta \dot r_T/v \\ \Delta \dot r_N/v \end{Bmatrix} = \begin{bmatrix} \Delta a/a & 0 & -\Delta e_X & -\Delta e_Y \\ \Delta u & -3\Delta a/2a & -2\Delta e_Y & +2\Delta e_X \\ 0 & 0 & -\Delta i_Y & +\Delta i_X \\ 0 & 0 & -\Delta e_Y & +\Delta e_X \\ -3\Delta a/2a & 0 & +2\Delta e_X & +2\Delta e_Y \\ 0 & 0 & +\Delta i_X & +\Delta i_Y \end{bmatrix} \times \begin{Bmatrix} 1 \\ u - u_0 \\ \cos u \\ \sin u \end{Bmatrix} \quad (13)$$

Here v denotes the orbital velocity in a circular orbit of radius a. A comparison with the analytical solution of the HCW equations[21]

exhibits a one-to-one correspondence of individual terms and underlines the mathematical equivalence of both formulations. The concepts of eccentricity and inclination relative vectors are deepened in the following section. It will be shown that $\Delta \boldsymbol{i}$ and $\Delta \boldsymbol{e}$ do not only provide an interesting geometrical interpretation of the relative motion, but also represent a powerful tool for formation-flying design.

Eccentricity/Inclination Vector Separation

Relative Eccentricity and Inclination Vectors

The linearized equations of relative motion (13) provide the relative Cartesian state vector $\Delta \boldsymbol{r}$ at any mean argument of latitude u (i.e., u is the independent variable) as a function of the relative orbital elements $\Delta \boldsymbol{e}$, $\Delta \boldsymbol{i}$, Δa and Δu at epoch t_0. Although Δa and Δu represent classical Keplerian elements differences, $\Delta \boldsymbol{e}$ and $\Delta \boldsymbol{i}$ deserve further reflections. Making use of the polar representation of the relative e/i vectors, Eqs. (4), (9), and (10) become

$$\Delta r_R/a = -\delta e \cos(u-\varphi) \tag{14}$$

$$\Delta r_T/a = 2\delta e \sin(u-\varphi) \tag{15}$$

$$\Delta r_N/a = \delta i \sin(u-\theta) \tag{16}$$

Thus, when not affected by differences Δa and Δu, the relative orbit of the spacecraft-2 with respect to spacecraft-1 is an ellipse of semimajor axis $2a\delta e$ in along-track direction and semiminor axis $a\delta e$ in radial direction (Fig. 4). While δe measures the size of the relative trajectory, the angle φ defines the relative pericenter. Whenever the argument of latitude u equals φ, spacecraft-2 is located right below the center. As soon as $u = \varphi + \pi/2$, spacecraft-2 takes over and is just ahead of the master satellite. In analogy with the preceding concepts, the relative inclination vector is used to describe the relative motion perpendicular to the orbital plane. The cross-track relative motion is described by a harmonic oscillation of amplitude $a\delta i$ and phase angle $u-\theta$.

Collision Avoidance

The concept of e/i vector separation has originally been developed for the safe collocation of geostationary satellites,[15] but can likewise be applied for proximity operations in LEO formations.[16] It is based on the consideration that the uncertainty in predicting the along-track separation of two spacecraft is generally much higher

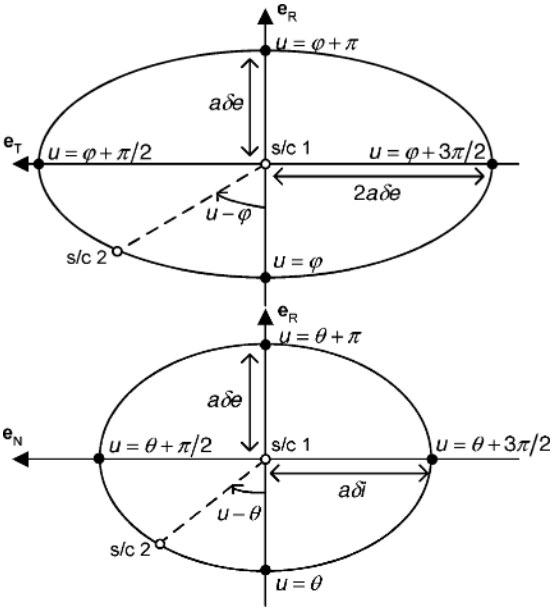

Fig. 4 Relative motion of two spacecraft with e/i vector separation: in-plane motion (top) and motion perpendicular to the flight direction (bottom).

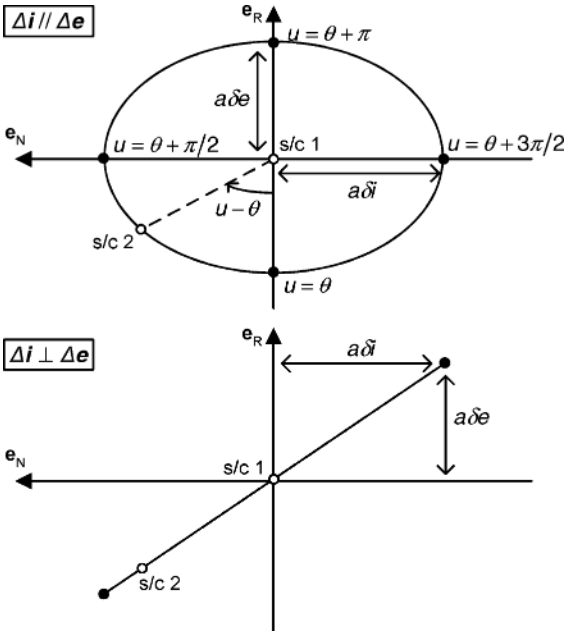

Fig. 5 Relative motion for parallel (top) and orthogonal (bottom) e/i vectors.

than for the radial and cross-track component. Because of the coupling between semimajor axis and orbital period, small uncertainties in the initial position and velocity result in a corresponding drift error and thus a secularly growing along-track error. Predictions of the relative motion over extended periods of time are therefore particularly sensitive to both orbit determination errors and maneuver execution errors.

To avoid a collision hazard in the presence of along-track position uncertainties, care must be taken to properly separate the two spacecraft in radial and cross-track direction.[22] As shown for GEO satellites,[15] this can be achieved by a parallel (or antiparallel) alignment of the relative e and i vectors. Even though these vectors are differently defined for near-equatorial, geostationary satellites, the convention adopted here ensures consistency with[15] and the same considerations are therefore applicable.

Parallel vectors $\Delta \boldsymbol{e}$ and $\Delta \boldsymbol{i}$ imply equality of the associated angles φ and θ. As illustrated before, $u = \varphi + k\pi$ with k integer (i.e., $k = 0, 1, \ldots$) mark the positions at which the two spacecraft exhibit their maximum radial separation; instead, $u = \varphi + (k + \frac{1}{2})\pi$ are the points of vanishing radial separation. Considering that $\varphi = \theta$ identifies the line of intersection of both orbital planes at which the cross-track separation vanishes, then $\Delta \boldsymbol{e} // \Delta \boldsymbol{i}$ ensures maximum Δr_R when $\Delta r_N = 0$ and vice versa, maximum Δr_N when $\Delta r_R = 0$. In contrast to this, the radial and cross-track separation can jointly vanish (i.e., $\Delta r_R = \Delta r_N = 0$) for orthogonal vectors $\Delta \boldsymbol{e} \perp \Delta \boldsymbol{i}$, which is risky in the presence of along-track position uncertainties (Fig. 5).

In the absence of a mutual drift ($\Delta a = 0$), the radial and cross-track separation are given by Eqs. (14–16). Thus for parallel relative e/i vectors the intersatellite distance is always ensured to be larger than $\min(a\delta e, a\delta i)$ even in the case of a vanishing along-track separation. In the case of drifting satellites, the radial offset has to be accounted as well. In general, this can be compensated by a suitably increased eccentricity vector separation.

Perturbed Relative Motion

Natural forces perturb the ideal, Keplerian satellite motion by introducing periodic and secular variations of the orbital elements. For formation-flying satellites operating in close proximity, the short-periodic perturbations are essentially cancelled, leaving long-periodic and secular changes of the relative e/i vectors. The relevant differential perturbations acting on a LEO formation arise from the asphericity of the Earth and from the aerodynamic drag. These variations have to be quantified to evaluate the stability of the

relative motion and investigate the necessity of a relative orbit control strategy.

Earth Oblateness Perturbations

The satellite orbits examined here are of relatively low altitude and are therefore fairly sensitive to perturbations because of the geopotential. The two principal gravitational effects caused by the Earth's equatorial bulge are the regression of the line of nodes and the rotation of the line of apsides, which mainly translate into short-periodic, long-periodic, and secular perturbations of the inclination and eccentricity vectors, respectively. The short-periodic (sp) oscillations are essentially related to the zonal terms of the geopotential, but the main effect is caused by the second-order zonal coefficient $J_2 = 1.082 \times 10^{-3}$ as follows[19]:

$$\delta \boldsymbol{e}_{\mathrm{sp}} = \frac{3}{2} J_2 \frac{R_\oplus^2}{a^2} \left\{ \begin{array}{l} (1 - 5/4 \sin^2 i) \cos u + (7/12 \sin^2 i) \cos 3u \\ (1 - 7/4 \sin^2 i) \sin u + (7/12 \sin^2 i) \sin 3u \end{array} \right\} \tag{17}$$

and

$$\begin{aligned} \delta i_{\mathrm{sp}} &= \tfrac{3}{8} J_2 \left(R_\oplus^2 \big/ a^2 \right) \sin(2i) \cos(2u) \\ \delta \Omega_{\mathrm{sp}} &= \tfrac{3}{4} J_2 \left(R_\oplus^2 \big/ a^2 \right) \cos(i) \sin(2u) \end{aligned} \tag{18}$$

Equations (17) and (18) provide an analytical tool for mapping the mean eccentricity and inclination vectors. In particular, by removing these perturbations from the osculating orbital elements, it is possible to evaluate the single averaged e/i vectors that exhibit only long-periodic and secular variations. To the order J_2, the short-periodic variations depend only on the argument of latitude, as shown by Eqs. (17) and (18). For short baselines, these effects can thus be neglected when forming the e/i vectors difference of two formation-flying spacecraft. Ignoring these perturbations, the relative eccentricity vector

$$\Delta \bar{\boldsymbol{e}} = \bar{\boldsymbol{e}}_2 - \bar{\boldsymbol{e}}_1 = \delta e \cdot \left\{ \begin{array}{l} \cos(\varphi_0 + \dot{\varphi} t) \\ \sin(\varphi_0 + \dot{\varphi} t) \end{array} \right\} \tag{19}$$

evolves along a circle of radius δe that is centered in the origin of the e-vector plane, with an angular velocity[19]

$$\dot{\varphi} = 2\pi / T_e \approx \tfrac{3}{2} (\pi / T) \left(R_\oplus^2 \big/ a^2 \right) J_2 (5 \cos^2 i - 1) \tag{20}$$

The period T_e of the relative e-vector motion is roughly 1000 times larger than the orbital period T. For sun-synchronous formations with orbital inclinations of 97–102 deg and associated altitudes of 500–1500 km, Eq. (20) yields a clockwise motion of $\Delta \bar{\boldsymbol{e}}$ with a period T_e of roughly 100–200 days.

The relative inclination vector

$$\Delta \bar{\boldsymbol{i}} = \left\{ \begin{array}{l} \Delta \bar{i}_X \\ \Delta \bar{i}_Y \end{array} \right\} = \left\{ \begin{array}{c} \Delta i_X \\ \Delta i_Y + \mathrm{d}(\Delta i_Y)/\mathrm{d}t \cdot t \end{array} \right\} \tag{21}$$

is likewise affected by J_2 perturbations that cause a secular shift of the orbital planes and thus a linear drift of Δi_Y given by[19]

$$\frac{\mathrm{d}}{\mathrm{d}t} \Delta i_Y \approx -\frac{3\pi}{T} J_2 \frac{R_\oplus^2}{a^2} \sin^2(i) \cdot \Delta i \tag{22}$$

for near circular orbits. The secular motion of the relative e/i vectors caused by the Earth oblateness is illustrated in Fig. 6. An initially parallel configuration will ultimately be destroyed unless correction maneuvers are performed to compensate for the natural drift of both vectors.

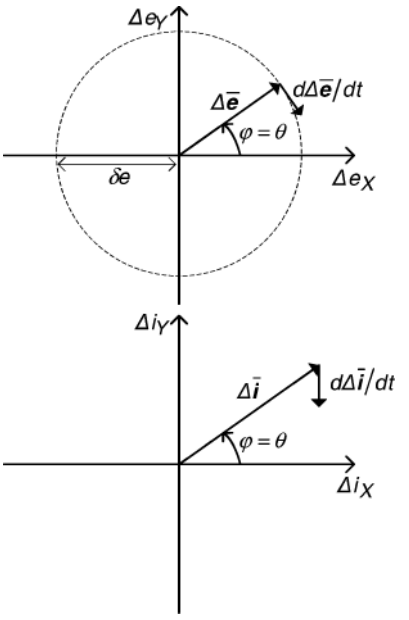

Fig. 6 Secular evolution of the relative eccentricity (top) and inclination vectors (bottom).

Nominal Formation-Flying Configuration

It can be recognized from Eqs. (21) and (22) that the absolute inclination of the formation-flying spacecraft should be identical ($\Delta i = 0$) to avoid a secular motion of the relative inclination vector. In this case, a separation of the two orbital planes by angle δi is achieved through a small offset in the right ascensions of their ascending nodes $\Delta \Omega = \pm \delta i / \sin i$. The resulting relative inclination vector has a phase angle $\theta = \pm \pi/2$, and the same (or opposite phase) must be selected for the relative eccentricity vector:

$$\Delta \boldsymbol{e} = \left\{ \begin{array}{c} 0 \\ \pm \delta e \end{array} \right\}, \qquad \Delta \boldsymbol{i} = \left\{ \begin{array}{c} 0 \\ \pm \delta i \end{array} \right\} \tag{23}$$

Such a choice for the nominal configuration provides a sort of passive stability to the formation because the secular Earth oblateness perturbations have minimum impact on the relative motion. The two orbital planes intersect near the poles ($u = \pm \pi/2$), and the spacecraft achieve the largest cross-track separation at the equator, and vice versa the radial separation vanishes at the equator crossing and is maximized near the poles, like that shown by Fig. 7. This provides the typical helix-shaped formation-flying configuration first introduced by Ref. 23 for advanced SAR applications.

Considering both safety and imaging constraints, the typical requirements for a SAR interferometry mission can be fulfilled by a formation with parallel relative e/i vectors. The interferometric technique is based on the stereoscopic effect that is induced by matching two SAR images obtained from two slightly different orbital positions. Whereas a differencing of SAR images obtained from two antennas separated in cross-track direction basically yields measurements of terrain elevations and therefore permits the derivation of digital elevation models (DEM), an adequate along-track separation provides measurements of the velocity of on-ground objects (e.g., for traffic monitoring, ocean currents, and glacier monitoring).

The height accuracy of interferometric images is determined by the so-called effective baseline.[24] The effective baseline is the distance B between the two planes spanned by the flight direction (along-track) and the target direction (antenna-beam-pointing direction) of the respective satellite (Fig. 7).

A larger effective baseline provides better height accuracies of the desired scene. On the other hand, small baselines ensure unambiguous retrieval of the height information with successful phase unwrapping. As a consequence, the formation-flying concept has to allow interferometric data acquisition with large and small baselines at a fixed baseline ratio.[7]

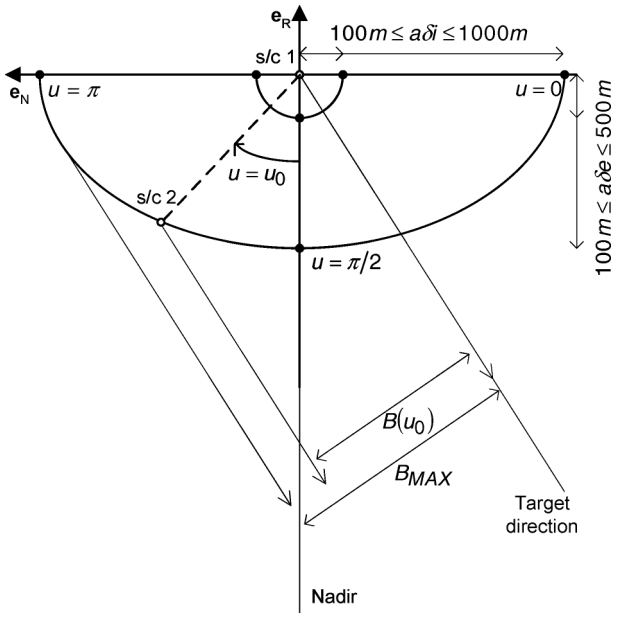

Fig. 7 Relative motion for different nominal cases and effective baseline.

Nominal relative orbital elements can be defined in accordance with the preceding considerations. The relative eccentricity modulus $a\delta e$ is limited by the minimum radial separation necessary for safe proximity operations (e.g., 100 m) and the maximum along-track separation required by SAR interferometry (e.g., 1 km). Similarly the relative inclination modulus $a\delta i$ is driven by the requirements on operational safety and effective baseline (e.g., 100 m–1 km). The relative semimajor axis Δa is nominally zero. It must be kept as small as possible to prevent an along-track drift. Finally, the relative argument of latitude Δu should nominally be zero and is limited by the maximum along-track separation for the formation. If necessary, a nonzero value of Δu could be selected to achieve a zero along-track separation at a specified argument of latitude. The resulting relative motion in cross-track and radial direction is illustrated in Fig. 7 for typical nominal cases, assuming positive angles $\varphi = \theta = \pi/2$.

Large Baselines and Longitude Swap Maneuvers

For large along-track separations, the modeling of short-periodic oscillations caused by the J_2 perturbations becomes crucial. A representative application is given by the aforementioned GRACE formation-flying mission, whose primary objective is the generation of Earth gravity field models with high spatial and temporal resolution. The twin satellites, named GRACE-1 and GRACE-2, measure their relative distance and its rate of change by a K-band microwave link with a typical accuracy of 1 μm/s. Following the injection on 17 March 2002, into a near-polar ($i = 89$ deg) circular orbit of 450 km altitude, regular orbit-keeping maneuvers are executed to maintain a relative along-track separation of 220 ± 50 km (Ref. 4). Mainly to balance the surface erosion of onboard K-band radar, both satellites have to exchange their position at least once during the mission lifetime. Such a position swap maneuver is planned to be done in the second half of 2005. To minimize the fuel expenditure and operations effort without sacrificing the mission safety, an e/i vector separation strategy has been selected for the implementation of the switching sequence.[16] As discussed in Ref. 16, the use of relative orbital elements is more appropriate in this context, because it allows the consideration of short-periodic perturbations. In view of that, Eq. (13) is preferred to the HCW Cartesian parameterization for planning longitude swap maneuvers with extended drift phases.

Throughout the period of interest, the relative inclination vector of the GRACE formation is located at a phase angle $\theta = 90$ deg, which implies that the two orbital planes intersect at the extreme orbital latitudes close to the north and south pole of the Earth. The relative inclination of about 33 μrad results in a maximum cross-track separation of 230 m that is attained near the equator crossing. In the absence of out-of-plane maneuver components, $\Delta \boldsymbol{i}$ remains unchanged during the longitude swap, and a parallel e/i vector configuration can only be achieved by proper orientation of the relative eccentricity vector. Because the osculating vector $\Delta \boldsymbol{e}$ matches the mean relative eccentricity vector $\Delta \bar{\boldsymbol{e}}$ for small along-track separations, it is appropriate to consider only the latter value in the drift maneuver planning. $\Delta \bar{\boldsymbol{e}}$ describes a circle of radius $\delta \bar{e} \approx 0.12 \times 10^{-3}$ about the origin, which is traversed in a period of $T_e = 94^d$ [compare Eq. (20)]. A parallel e/i vector configuration is naturally achieved on 7 September and 9 December 2005, whereas $\Delta \bar{\boldsymbol{e}}$ and $\Delta \bar{\boldsymbol{i}}$ are antiparallel on 23 July and 24 October 2005. These dates therefore represent an optimum choice for the instance at which GRACE-2 passes GRACE-1 during the longitude swap sequence. The computation of the drift start maneuver date is straightforward from the time of optimum flyby and the desired total drift duration.

Differential Drag

The interaction of the upper atmosphere with the satellite's surface produces the dominant environmental disturbance for LEO spacecraft. The main force caused by the impact of atmospheric molecules on the spacecraft surface is antiparallel to the velocity of the spacecraft relative to the incident stream and is named aerodynamic drag. The along-track satellite acceleration

$$|\ddot{r}_D| = \tfrac{1}{2} \rho v^2 \cdot C_D (A/m) \tag{24}$$

caused by drag is determined by the atmospheric density ρ, the orbital velocity v, and the ballistic coefficient (i.e., the effective area-to-mass ratio)

$$b = C_D (A/m) \tag{25}$$

Here, A is the satellite's cross-section area, m is the satellite mass, and C_D is the aerodynamic drag coefficient. As a preliminary approximation, density variations over distances of less than a kilometer can be neglected. Thus, the relative along-track acceleration for two formation-flying spacecraft is driven by the differences in their ballistic coefficients $\varepsilon = (b_2 - b_1)/b_1$. This causes an accumulated along-track offset

$$\Delta r_T = \tfrac{1}{2} \varepsilon \, |\ddot{r}_D| \cdot \Delta t^2 \tag{26}$$

over a time interval Δt, which has to be compensated to maintain the nominal formation-flying configuration. The impact of differential drag can be minimized using identical design for the participating satellites. In such a way the ballistic coefficients can be matched to roughly 1% (Ref. 25) at launch. Assuming that mass variations during the mission lifetime can contribute an additional estimated difference of 1%, an offset $\varepsilon = 2\%$ can be adopted for a realistic operational scenario. According to the Harris–Priester model,[26] the atmospheric density at a representative altitude of 500 km amounts to 1 g/km^3 for mean solar flux conditions. At a ballistic coefficient $b_1 = 0.006$ m^2/kg and an orbital velocity $v = 7.6$ km/s, Eq. (26) yields an along-track offset of 5 cm within one orbital revolution and a 10-m offset after one day. Even though these values might increase by a factor of 10 during high solar activities and geomagnetic storms, differential drag has evidently modest impact on the formation control during nominal operations even for LEO orbits.

On the other hand, this conclusion is no longer valid if one of the two spacecraft enters a safe mode with uncontrolled yaw angle. Depending on the specific geometry, the effective cross section might increase and thus cause large differential drag accelerations of several hundred nm/s^2. When lasting over extended periods of time, a safe mode can thus cause notable change in along-track separation.[27] However, given the fact that no science data can be collected in safe mode and considering the collision protection provided by the e/i vector separation, the undesired changes of the relative orbit is considered noncritical from a mission operations point of view. The nominal formation configuration can always be

restored by a series of corrective maneuvers performed either autonomously or with ground intervention after the end of the safe mode.

Relative Orbit Control

A relative orbit control system is necessary either to maintain the nominal formation geometry over the mission lifetime (i.e., station-keeping) or to reconfigure the formation to realize certain specific objectives. In both cases correction maneuvers have to be planned and executed to ensure conformance with predefined target relative orbital elements (Δa^t, $\Delta \boldsymbol{e}^t$, $\Delta \boldsymbol{i}^t$, Δu^t). Here we consider an operational scenario with two formation-flying spacecraft. While the master satellite is passive from a relative orbit control point of view, the chaser is performing relative orbit correction maneuvers. The inversion of our linearized relative motion model (13) provides the following system of equations

$$\begin{Bmatrix} Da \\ De_X \\ De_Y \\ Di_X \\ Di_Y \\ Du \end{Bmatrix} = \frac{1}{v} \begin{bmatrix} 0 & 2a & 0 \\ \sin u & 2\cos u & 0 \\ -\cos u & 2\sin u & 0 \\ 0 & 0 & \cos u \\ 0 & 0 & \sin u \\ 0 & -3v/a \cdot \Delta t & 0 \end{bmatrix} \begin{Bmatrix} \Delta v_R \\ \Delta v_T \\ \Delta v_N \end{Bmatrix} \tag{27}$$

commonly known as the simplified Gauss equations,[19] adapted to near-circular nonequatorial orbits. It provides the relationships between the velocity changes Δv_R, Δv_T, and Δv_N and the desired orbital corrections (Da, $D\boldsymbol{e}$, $D\boldsymbol{i}$, Du) and can thus be used to solve the maneuver planning problem. Equation (27) shows that for a given thrust, located at a specific mean argument of latitude u, instantaneous variations of the actual relative orbital elements $\Delta \boldsymbol{e}$, $\Delta \boldsymbol{i}$, and Δa are generated, as well as a net change of Δu within a time interval Δt. As expected, the control problem is decoupled. Whereas a thrust in cross-track direction affects only the relative inclination vector, a thrust in the orbital plane (i.e., along-track and radial directions) influences the relative eccentricity vector, the relative semimajor axis, and the derivative of the relative argument of latitude. Because of their double efficiency in terms of propellant consumption, only along-track maneuvers are used to control the relative eccentricity vector. In the general case two symmetric thrusts (indicated by the superscripts 1 and 2) in positive and negative tangential directions are necessary and sufficient to maintain the target relative elements and control the in-plane relative motion. The solution is given by

$$\begin{aligned} \Delta v_T^1 &= +(v/4)(\|D\boldsymbol{e}\| + Da/a) \\ \Delta v_T^2 &= -(v/4)(\|D\boldsymbol{e}\| - Da/a) \end{aligned} \tag{28}$$

for the maneuver sizes and

$$u^1 = \operatorname{atan}(De_Y/De_X), \qquad u^2 = u^1 + \pi \tag{29}$$

for the respective locations. The desired orbital corrections are calculated as the difference ($Da = \Delta a^t - \Delta a$, $D\boldsymbol{e} = \Delta \boldsymbol{e}^t - \Delta \boldsymbol{e}$) between target and actual relative orbital elements. More specifically the relative orbital elements are evaluated as mean relative elements in which the J_2-short-periodic perturbations have been removed [see Eqs. (17) and (18)].

Adopting the parallel e/i vector separation given by Eq. (23) as the nominal target configuration with a relative perigee at $\varphi = \pi/2$, the derivative of the relative eccentricity vector is always directed along the positive e_X axis. It can thus be counteracted by performing along-track maneuvers in the vicinity of the ascending and descending nodes of the orbit [as from Eq. (29)]. Given a representative period $T_e = 100$ days of the J_2-induced perigee variation for sun-synchronous formations (i.e., at 500 km altitude), the daily shift of the relative eccentricity vector amounts to

$$D\boldsymbol{e} = -\frac{\mathrm{d}\Delta \boldsymbol{e}}{\mathrm{d}t} \cdot 1d = -\delta e \begin{Bmatrix} 2\pi/T_e \\ 0 \end{Bmatrix} \cdot 1d \approx -\delta e \begin{Bmatrix} 0.06 \\ 0 \end{Bmatrix} \tag{30}$$

where δe is the relative eccentricity. To compensate this motion, Eq. (28) gives a daily along-track velocity increment of

$$|\Delta v_T| = \left|\Delta v_T^1\right| + \left|\Delta v_T^2\right| = (v/2)\|D\boldsymbol{e}\| \approx (3 \times 10^{-5})(a\delta e)/\mathrm{s} \tag{31}$$

that is directly proportional to the nominal eccentricity offset. Considering the typical eccentricity separation range $a\delta e = 100$ m... 500 m, a total Δv of 0.3...1.5 cm/s is thus required each day to maintain the nominal relative perigee.

The correction of the relative mean argument of latitude is a straightforward application of Eqs. (27) and (28). Additional burns are not necessary if the eccentricity control maneuvers are also used for the along-track separation control. The magnitudes of thrusts 1 and 2 in Eq. (28) are adjusted to introduce the desired longitude drift

$$D\dot{u} = Du/T_M \tag{32}$$

where T_M is the time between each maneuver pair (i.e., the maneuver cycle for eccentricity control). In such a way the mean along-track separation of the formation can be confined within a longitude window (i.e., $-\Delta u_{\mathrm{MAX}} < \Delta u < +\Delta u_{\mathrm{MAX}}$) whose minimum size is dictated by the temporary semimajor offset introduced by the individual eccentricity control maneuvers.

Relative orbit control maneuvers in cross-track direction are not necessary for the nominal parallel e/i vector separation, but corrections of the relative inclination vector could become useful in the case of reconfigurations of the formation (e.g., changes of the effective baseline for SAR interferometry). In this case the solution consists in a single burn in cross-track direction given by Eq. (27):

$$\Delta v_N = v\|D\boldsymbol{i}\|, \qquad u = \operatorname{atan}(Di_Y/Di_X) \tag{33}$$

The overall strategy for the maintenance of the formation appears very simple and could be adopted either for a ground-in-the-loop control system or for an autonomous implementation. The method will be applied in the following sections to a relevant study case, and, finally, nonlinear numerical simulations will validate the analytical treatment.

Study Case: TanDEM-X/TerraSAR-X Formation

TerraSAR-X (TSX) is an advanced SAR-satellite system for scientific and commercial applications. The satellite has a size of 5×2.4 m, a mass of 1200 kg, and carries a high-resolution SAR operating in the X-band (9.65 GHz). A Russian DNEPR-1 rocket launched from Baikonour, Kazakhstan, will inject TSX into a 514-km sun-synchronous dusk-dawn orbit with 97-deg inclination and an 11-day repeat period. Presently the spacecraft is under integration phase, and the launch is scheduled for May 2006. TSX is planned to be operated for a period of five years and will therefore provide SAR data on a long-term, operational basis. The German Space Operation Center will provide the mission operations segment using ground stations at Weilheim and Neustrelitz.

As a complement to TerraSAR-X, the TanDEM-X (TDX) mission has recently been proposed in a contest for new Earth observation missions within the German national space program.[17] It involves a second spacecraft, which is almost identical to TSX and shall likewise be operated for five years. The two spacecraft will fly in a precisely controlled formation to form a radar interferometer with typical baselines of 1 km. This allows a much higher resolution than achievable in the X-SAR/SRTM shuttle topography mission and thus the generation of DEMs with unrivaled accuracy.

Formation-Flying Concept

To maintain the nominal orbital configuration of the TDX/TSX formation, regular maneuvers will have to be executed by the TDX spacecraft. Primarily, these maneuvers must compensate for changes of the relative orbit caused by TSX orbit-keeping maneuvers and changes of the relative orbit caused by the Earth oblateness. In addition, occasional maneuvers might be required to intentionally change the relative orbit (e.g., to achieve different effective baselines for SAR interferometry) or to restore the nominal configuration after a contingency.

Routine orbit-keeping maneuvers are performed on TSX to ensure that the actual spacecraft orbit deviates by less than 250 m (perpendicular to the flight direction) from a predefined Earth-fixed reference trajectory.[28] Aside from compensating semimajor axis changes caused by atmospheric drag, these maneuvers maintain a near-frozen eccentricity vector for TSX. Depending on solar activity, the size and frequency of TSX orbit-keeping maneuvers vary between 1 cm/s about once per week near the start of mission and 5 cm/s approximately once per day near the end of life.[29]

Given the fact that a 5-cm/s along-track maneuver changes the semimajor axis by 100 m and thus introduces a drift of 1000 m per revolution (or 15 km/d), it is evident that TDX is required to perform closely synchronized orbit-keeping maneuvers for maintaining the TSX/TDX formation geometry. Ideally, TSX maneuvers should be duplicated by TDX, in which case the relative orbital elements of both spacecraft will not be affected.

On top of duplicating TSX maneuvers, the TDX spacecraft will be required to perform corrective maneuvers for maintaining the relative eccentricity vector (against geopotential perturbations) and the relative argument of latitude (against differential drag effects).

Numerical Simulation

The objective of this section is to validate the presented analytical assessments and demonstrate the feasibility of the proposed orbit control concept. In particular the TDX/TSX formation is chosen as test bed, and a representative nominal configuration is simulated over a 30-day time interval under real-world dynamics.

A comprehensive dynamic model for the acceleration of an Earth-orbiting spacecraft under the action of gravitational and nongravitational forces is adopted. It comprises the Earth gravity model GGM01S up to order and degree 40, the luni-solar third-body gravitational perturbation, the luni-solar Earth tides among the mass forces, the atmospheric drag (Jacchia–Gill density model), and the solar radiation pressure among the surface forces. All models are supplemented by up-to-date Earth rotation parameters and solar/geomagnetic data. The force model is used in combination with a numerical integration of first-order differential equations to predict the spacecraft orbits. The main parameters of the force model for TSX (i.e., s/c-1) are the drag coefficient $C_D = 2.3$, its reference surface $A = 3.2$ m^2, and the satellite mass $m = 1238.0$ kg. Apart from a difference in the ballistic coefficient given by $\varepsilon = 2\%$, TDX (i.e., s/c-2) is assumed to be an identical replication of TSX.

First of all, an initial nominal configuration is selected for the TDX/TSX formation flying. This is given by Eq. (23) as

$$\Delta a = 0, \qquad \Delta u = 0, \qquad a\Delta \boldsymbol{e} = \left\{ \begin{array}{c} 0 \\ +300 \text{ m} \end{array} \right\}$$

$$a\Delta \boldsymbol{i} = \left\{ \begin{array}{c} 0 \\ -1000 \text{ m} \end{array} \right\} \tag{34}$$

with $a = 6892.945$ km. The formation is initialized by adding the relative nominal elements (34) to the mean TSX elements at the initial epoch t_0 in May 2006. Input to the simulation scenario is the a priori TSX maneuver planning. It consists of in-plane and out-of-plane maneuvers (i.e., size/direction of velocity corrections and time of execution) performed to control the TSX osculating orbit within 250 m distance from the target trajectory. A numerical propagation of the TDX/TSX orbits, including the aforementioned orbit-keeping maneuvers, identically reproduced by TDX, provides the natural uncontrolled relative motion over 30 days (Figs. 8 and 9).

As expected, the relative eccentricity vector draws a circle-arc in the e-vector plane, while the relative inclination vector is nearly constant because of the relative perigee at 90 deg (Fig. 8). The formation-flying configuration evolves from a safe parallel separation of the e/i vectors at time t_0 to a perpendicular orientation after 25 days [compare Eq. (20)]. As shown by Fig. 9, this is dangerous because radial and cross-track separations vanish at the same time. A relative orbit control is necessary to stabilize the formation. To this purpose, symmetric tangential maneuvers are performed by TDX

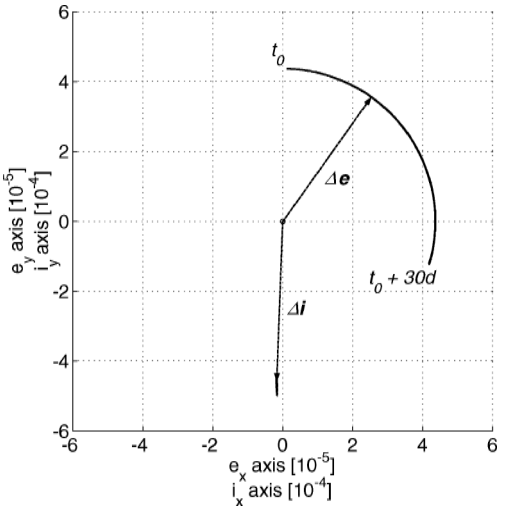

Fig. 8 Mean relative e/i vector motion over 30 days.

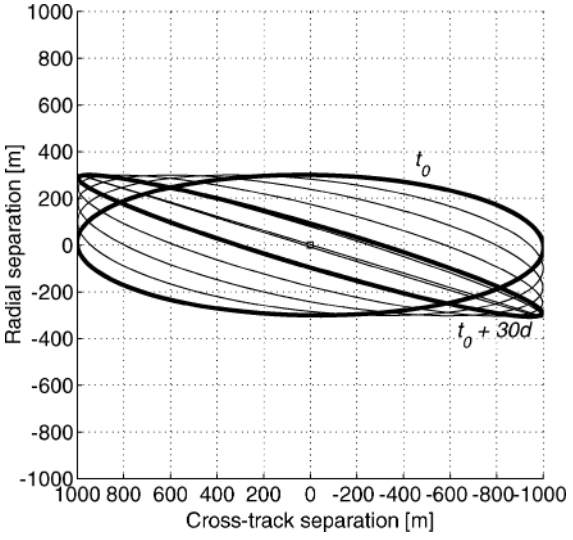

Fig. 9 Osculating motion of TDX with respect to TSX in cross-track and radial directions (only one revolution every five days is shown).

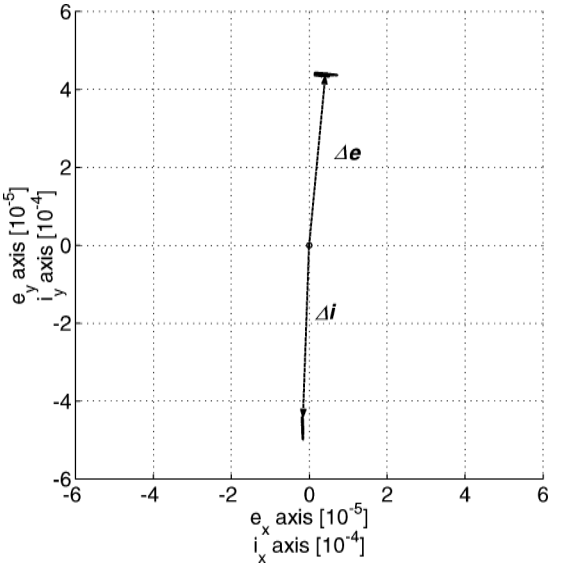

Fig. 10 Controlled relative e/i vector motion over 30 days.

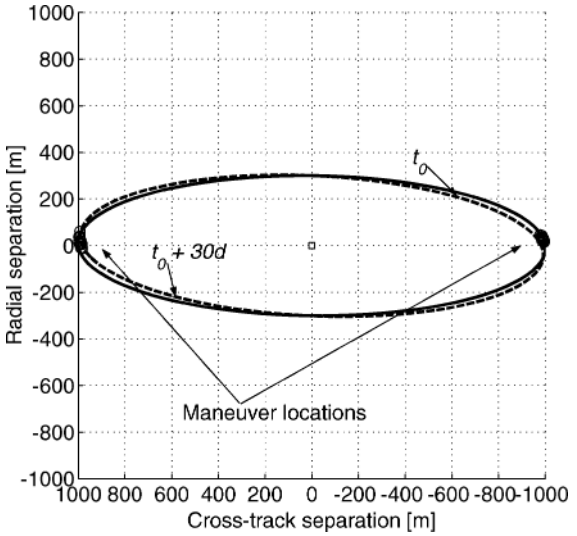

Fig. 11 Controlled osculating motion of TDX with respect to TSX in cross-track and radial directions (first and last revolution) and TDX maneuver locations.

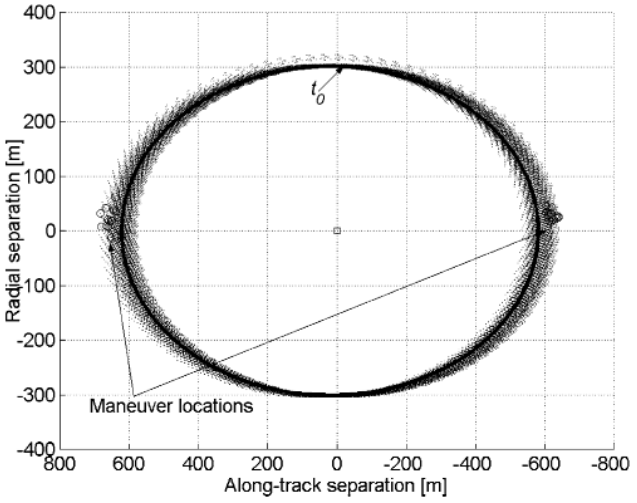

Fig. 12 Controlled osculating motion of TDX with respect to TSX in along-track and radial directions and maneuver locations.

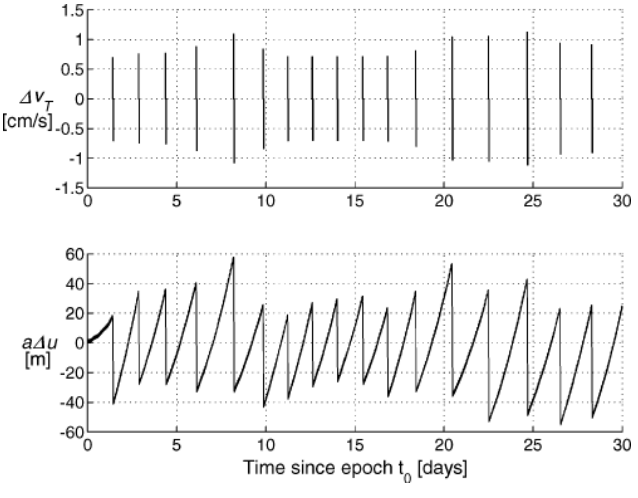

Fig. 13 Size of tangential maneuvers (top) and relative mean argument of latitude (bottom) over 30 days.

near the nodes. The maneuver execution is triggered by the violation of an arbitrary threshold of 7 deg imposed to the angle formed by the relative eccentricity and inclination vectors (i.e., $\varphi - \theta \leq 7$ deg). Figure 10 shows the controlled e/i vector parallel orientation over the simulation time interval.

The longitude drift induced by differential drag is balanced by a proper adjustment of the maneuver pairs. The maneuvers size and exact location are computed using Eqs. (28–32), in order to maintain the relative argument of latitude within a longitude window given by $\Delta u_{\mathrm{MAX}} = 60$ m. Figures 11 and 12 depict the controlled osculating relative motion of TDX in the orbital frame of TSX. As anticipated, a daily maneuver budget of 1 cm/s is necessary to control the relative eccentricity vector, while the velocity corrections induced by differential drag effects are negligible (Fig. 13). The time interval between maneuver pairs amounts to two days; this is straightforward if one considers that the relative eccentricity vector rotates by an angle of 7 deg within roughly two days (i.e., $\dot{\varphi} \approx 360 \text{ deg}/100d$).

Conclusions

Although using the Hill frame coordinates is a common method to describe the satellites relative motion, they have the distinct disadvantage that for a general orbit their differential equations must be solved to obtain the precise instantaneous geometry of the formation. Because of this fact, in this paper a description in terms of Keplerian relative elements has been preferred to the canonical Cartesian parameterization. In contrast to the fast varying Hill–Clohessy–Wiltshire variables, the use of orbital elements differences simplifies the formation-flying description and the satellite relative position computation.

Various sets of relative orbital elements have been proposed in the past decades in the frame of formation-flying dynamics and control, but actually the most intuitive, straightforward representation in terms of relative eccentricity and inclination vectors has never been investigated for formation-flying design in low Earth orbit. This paper generalizes the method of eccentricity/inclination vector separation, first developed for the safe collocation of geostationary satellites, and extends its application to proximity operations of formation-flying spacecraft.

The spontaneous geometrical representation offers a direct correlation between the relevant characteristics of the bounded relative motion in near circular orbit and the magnitude/phase of the relative eccentricity/inclination vectors. This aspect extremely simplifies the design of safe, passively stable formation-flying configurations. In particular, minimum collision risk conditions can be guaranteed by imposing the (anti-)parallelism of the eccentricity and inclination vectors of the respective satellites, while J_2-stable relative orbits are obtained by setting a specific nominal phase for the configuration.

The new approach is shown to be suitable either for the realization of synthetic aperture radar interferometers with baselines below 1 km or the application in longitude swap operations with along-track separations above 200 km. In the first case an active relative orbit control strategy is necessary, in order to compensate for the main disturbance forces represented by Earth's oblateness perturbations and differential aerodynamic drag. The proposed strategy is based on the eccentricity/inclination vectors control and makes use of pairs of pulses separated by half a revolution in velocity and antivelocity directions. It appears very simple and could be used for a ground-in-the-loop control system as well as for an autonomous onboard implementation. The required velocity budget for relative orbit control has been expressed in terms of relative orbital elements. It is directly proportional to the relative eccentricity offset and amounts to a daily 0.3 . . . 1.5 cm/s for a typical quasipolar formation at 500 km altitude with 100 m. . . 500 m eccentricity separation. In the second case, a passive control strategy has been studied. Taking care of the natural evolution of the relative orbital elements of the participating satellites, optimum maneuver dates are identified for the reconfiguration of the GRACE formation. By proper timing of the maneuvers, a safe limit for the minimum distance during the encounter can be guaranteed.

Overall, the paper focuses on realistic application cases closely related to upcoming formation-flying missions. The intention is to propose a practical and reliable way to formation flying: a technology that is discussed and studied since decades but is still confined in research laboratories. Real-world simulations confirm the analytical assessment and show that simple techniques, which exploit the natural orbital motion to full extent, can meet the demanding requirements of long-term close formation flying.

Acknowledgments

This study has been motivated by the TanDEM-X Phase-A study proposal, realized in public–private partnership by DLR e.V. and Astrium EADS GmbH, within the German national space program. The authors would like to thank the Microwaves and Radar Institute for the useful technical discussions.

References

[1]Mclaughlin, C. A., Alfriend, K. T., and Lovell, T. A., "Analysis of Reconfiguration Algorithms for Formation Flying Experiments," International Symposium on Formation Flying Missions and Technologies, Nov. 2002.

[2]Bristow, J., Folta, D., and Hartman, K., "A Formation Flying Technology Vision," AIAA Paper 2000-5194, Sept. 2000.

[3]Scharf, D. P., Hadaegh, F. Y., and Kang, B. H., "A Survey of Spacecraft Formation Flying Guidance," International Symposium On Formation Flying Missions and Technologies, Nov. 2002.

[4]Kirschner, M., Montenbruck, O., and Bettadpur, S., "Flight Dynamics Aspects of the GRACE Formation Flying," International Symposium On Space Flight Dynamics, 2001.

[5]Folta, D., and Hawkings, A., "Results of NASA's First Autonomous Formation Flying Experiment: Earth-Observing-1 (EO-1)," AIAA Paper 2002-4743, Aug. 2002.

[6]Inalhan, G., Tillerson, M., and How, J. P., "Relative Dynamics and Control of Spacecraft Formations in Eccentric Orbits," *Journal of Guidance, Control, and Dynamics*, Vol. 25, No. 1, 2002, pp. 48–59.

[7]Fiedler, H., and Krieger, G., "Close Formation Flight of Passive Receiving Micro-Satellites," International Symposium On Space Flight Dynamics, Paper 1030, Oct. 2004.

[8]Kong, E. M. C., Miller, D. W., and Sedwick, R. M., "Exploiting Orbital Dynamics for Aperture Synthesis Using Distributed Satellite Systems: Applications to a Visible Earth Imager System," *Journal of Astronautical Sciences*, Vol. 47, No. 1, 1999, pp. 53–75.

[9]Clohessy, W. H., and Wiltshire, R. S., "Terminal Guidance System for Satellite Rendezvous," *Journal of Aerospace Science*, Vol. 27, No. 9, 1960, pp. 653–658.

[10]Sabol, C., Burns, R., and McLaughlin, C. A., "Formation Flying Design and Evolution," *Journal of Spacecraft and Rockets*, Vol. 38, No. 2, 2001, pp. 270–278.

[11]Schweighart, S., and Sedwick, R., "High-Fidelity Linearized J2 Model for Satellite Formation Flight," *Journal of Guidance, Control, and Dynamics*, Vol. 25, No. 6, 2002, pp. 1073–1080.

[12]Schaub, H., and Alfriend, K. T., "J2 Invariant Relative Orbits for Spacecraft Formations," Flight Mechanics Symposium, NASA, Greenbelt, MD, May 1999.

[13]Kasdin, N. J., and Kolemen, E., "Bounded, Periodic Relative Motion Using Canonical Epicyclic Orbital Elements," American Astronautical Society, Paper 05-186, Jan. 2005.

[14]Gim, D., and Alfriend, K. T., "The State Transition Matrix of Relative Motion for the Perturbed Non-Circular Reference Orbit," American Astronautical Society, Paper 01-222, Feb. 2001.

[15]Eckstein, M. C., Rajasingh, C. K., and Blumer, P., "Colocation Strategy and Collision Avoidance for the Geostationary Satellites at 19 Degrees West," International Symposium on Space Flight Dynamics, 1989.

[16]Montenbruck, O., Kirschner, M., and D'Amico, S., "E-/I-Vector Separation for GRACE Proximity Operations," DLR/German Space Operations Center, TN 04-08, Oberpfaffenhofen, Germany, 2004.

[17]Moreira, A., et al., "TanDEM-X: A TerraSAR-X Add-on Satellite for Single-Pass SAR Interferometry," Geoscience and Remote Sensing Society, International Geoscience and Remote Sensing Symposium, 2004.

[18]Gill, E., "Description of Keplerian Relative Motion in an Orbital Reference Frame," DLR/German Space Operations Center, TN 02-02, Oberpfaffenhofen, Germany, 2002.

[19]Micheau, P., "Orbit Control Techniques for Low Earth Orbiting (LEO) Satellites," *Spaceflight Dynamics*, Cepadues-Editions, edited by J. P. Carrou, Toulouse, France, 1995, Chap. 13.

[20]Jarnagin, M. P., Jr., "Expansions in Elliptic Motion," *Astronomical Papers of the American Ephemeris*, Vol. 18, Nautical Almanac Office, U.S. Naval Observatory, Washington, DC, 1965.

[21]Schaub, H., and Junkins, J. L., "Spacecraft Formation Flying," *Analytical Mechanics of Space Systems*, AIAA Education Series, AIAA, Reston, VA, 2003, Chap. 14.

[22]Fiedler, H., "Analysis of TerraSAR-L Cartwheel Constellations, TerraSAR-L ESA-Study," DLR-TN, Oberpfaffenhofen, Germany, Nov. 2003.

[23]Moreira, A., Krieger, G., and Mittermayer, J., U.S. Patent 6,677,884 B2, Jan. 2004.

[24]Hanssen, R. F., *Radar Interferometry—Data Interpretation and Error Analysis*, Kluwer Academic, Boston, 2001, p. 35.

[25]Kirschner, M., "First Results on the Implementation of the GRACE Formation," 3rd International Workshop on Satellite Constellations and Formations, Center of Studies and Activities for Space "G. Colombo," Pisa, Italy, Feb. 2003.

[26]Montenbruck, O., and Gill, E., *Satellite Orbits—Models, Methods, and Applications*, Springer-Verlag, Heidelberg, Germany, 2000, p. 91.

[27]Feucht, U., Nitsch, A., and Wagner, O., "Attitude Impact on the GRACE Formation Orbit," 3rd International Workshop on Satellite Constellations and Formations, Center of Studies and Activities for Space "G. Colombo," Pisa, Italy, Feb. 2003.

[28]D'Amico, S., Arbinger, Ch., Kirschner, M., and Campagnola, S., "Generation of an Optimum Target Trajectory for the TerraSAR-X Repeat Observation Satellite," 18th International Symposium On Space Flight Dynamics, Paper 1044, Oct. 2004.

[29]Arbinger, Ch., D'Amico, S., and Eineder, M., "Precise Ground-in-the-Loop Orbit Control for Low Earth Observation Satellites," 18th International Symposium On Space Flight Dynamics, Paper 1035, Oct. 2004.